PRAMANA
— journal of
physics

Vol. 66, No. 4
April 2006
pp. 731–752

Chiral dynamics of baryon resonances and hadrons in a nuclear medium

E OSET[1], D CABRERA[1], V K MAGAS[1], L ROCA[1], S SARKAR[1],
M J VICENTE VACAS[1] and A RAMOS[2]
[1]Departamento de Física Teórica and IFIC, Centro Mixto Universidad de Valencia-CSIC, Institutos de Investigación de Paterna, Apdo. Correos 22085, 46071, Valencia, Spain
[2]Departament d'Estructura i Constituents de la Matéria, Universitat de Barcelona, Diagonal 647, 08028 Barcelona, Spain
E-mail: oset@ific.uv.es

Abstract. In these lectures I make an introduction to chiral unitary theory applied to the meson–baryon interaction and show how several well-known resonances are dynamically generated, and others are predicted. Two very recent experiments are analyzed, one of them showing the existence of two $\Lambda(1405)$ states and the other one providing support for the $\Lambda(1520)$ resonance as a quasi-bound state of $\Sigma(1385)\pi$. The use of chiral Lagrangians to account for the hadronic interaction at the elementary level introduces a new approach to deal with the modification of meson and baryon properties in a nuclear medium. Examples of it for $\bar{K}$, η and ϕ modification in the nuclear medium are presented.

Keywords. Chiral unitary theory; hadron physics; hadrons in a medium.

PACS Nos 11.30.Rd; 11.30.-a; 25.80.Nv; 24.10.Eq; 24.80.+y; 25.20.-x

1. Introduction

Nowadays it is commonly accepted that QCD is the theory of strong interactions, with quarks as building blocks for baryons and mesons, and gluons as mediators of the interaction. However, at low energies typical of the nuclear phenomena, perturbative calculations with the QCD Lagrangian are not possible and one has to resort to other techniques to use the information of the QCD Lagrangian. One of the most fruitful approaches has been the use of chiral perturbation theory, χPT [1]. The theory introduces effective Lagrangians which involve only observable particles, mesons and baryons, respects the basic symmetries of the original QCD Lagrangian, particularly chiral symmetry, and organizes these effective Lagrangians according to the number of derivatives of the meson and baryon fields.

The introduction of unitarity constraints in coupled channels in chiral perturbation theory has led to unitary extensions of the theory and starting from the same effective Lagrangians allow one to make predictions at much higher energies. One

of the interesting consequences of these extensions is that they generate dynamically low-lying resonances, both in the mesonic and baryonic sectors. By this we mean that they are generated by the multiple scattering of the meson or baryon components, much the same way as the deuteron is generated by the interaction of the nucleons through the action of a potential, and they are not pre-existent states that remain in the large N_c limit where the multiple scattering is suppressed.

2. Baryon–meson interaction

The interaction of the octet of stable baryons with the octet of pseudoscalar mesons is given to lowest order by the Lagrangian [2,3]

$$\mathcal{L}_1 = \langle \bar{B} i\gamma^\mu \bigtriangledown_\mu B\rangle - M_B\langle \bar{B}B\rangle + \frac{1}{2}D\langle \bar{B}\gamma^\mu\gamma_5 \{u_\mu, B\}\rangle + \frac{1}{2}F\langle \bar{B}\gamma^\mu\gamma_5[u_\mu, B]\rangle \tag{1}$$

$$\begin{aligned} &\nabla_\mu B = \partial_\mu B + [\Gamma_\mu, B],\\ &\Gamma_\mu = \frac{1}{2}(u^+\partial_\mu u + u\partial_\mu u^+),\\ &U = u^2 = \exp(i\sqrt{2}\Phi/f),\\ &u_\mu = iu^+\partial_\mu U u^+, \end{aligned} \tag{2}$$

where the symbol $\langle\ \rangle$ stands for the trace of the matrices and the $SU(3)$ matrices for the meson and the baryon fields are given by

$$\Phi = \begin{pmatrix} \frac{1}{\sqrt{2}}\pi^0 + \frac{1}{\sqrt{6}}\eta & \pi^+ & K^+ \\ \pi^- & -\frac{1}{\sqrt{2}}\pi^0 + \frac{1}{\sqrt{6}}\eta & K^0 \\ K^- & \bar{K}^0 & -\frac{2}{\sqrt{6}}\eta \end{pmatrix}, \tag{3}$$

$$B = \begin{pmatrix} \frac{1}{\sqrt{2}}\Sigma^0 + \frac{1}{\sqrt{6}}\Lambda & \Sigma^+ & p \\ \Sigma^- & -\frac{1}{\sqrt{2}}\Sigma^0 + \frac{1}{\sqrt{6}}\Lambda & n \\ \Xi^- & \Xi^0 & -\frac{2}{\sqrt{6}}\Lambda \end{pmatrix}. \tag{4}$$

At lowest order in momentum, that we will keep in our study, the interaction Lagrangian comes from the Γ_μ term in the covariant derivative and we find

$$L_1^{(B)} = \left\langle \bar{B} i\gamma^\mu \frac{1}{4f^2}[(\Phi\partial_\mu\Phi - \partial_\mu\Phi\Phi)B - B(\Phi\partial_\mu\Phi - \partial_\mu\Phi\Phi)] \right\rangle \tag{5}$$

which leads to a common structure of the type $\bar{u}\mu^u(k_\mu + k'_\mu)u$ for the different channels, where $u, \bar{u}$ are the Dirac spinors and k, k' the momenta of the incoming and outgoing mesons.

We take the K^-p state and all those that couple to it within the chiral scheme. These states are $\bar{K}^0 n, \pi^0\Lambda, \pi^0\Sigma^0, \pi^+\Sigma^-, \pi^-\Sigma^+, \eta\Lambda, \eta\Sigma^0, K^+\Xi^-, K^0\Xi^0$. Hence we

have a problem with ten coupled channels. We should notice that, in addition to the six channels considered in [4] one has the two η channels, $\eta\Lambda$ and $\eta\Sigma^0$ and the two K channels, $K^+\Xi^-$ and $K^0\Xi^0$. Although these channels are above threshold for K^-p scattering at low energies, they couple strongly to the K^-p system and there are important interferences between the real parts of the amplitudes, which make their inclusion in the coupled-channel approach very important.

The lowest-order amplitudes for these channels are easily evaluated from eq. (5) and are given by

$$V_{ij} = -C_{ij}\frac{1}{4f^2}\bar{u}(p')\gamma^\mu u(p)(k_\mu + k'_\mu), \tag{6}$$

where $p, p'(k, k')$ are the initial and final momenta of the baryons (mesons). Also, for low energies one can safely neglect the spatial components in eq. (6) and only the γ^0 component becomes relevant, hence simplifying eq. (6) we get

$$V_{ij} = -C_{ij}\frac{1}{4f^2}(k^0 + k'^0) \tag{7}$$

with C_{ij} $SU(3)$ coefficients, which are easily derived from the chiral Lagrangians [5].

3. Unitarized chiral perturbation theory: N/D or dispersion relation method

One can find a systematic and easily comprehensible derivation of the ideas of the N/D method applied for the first time to the meson–baryon system in [6], which we reproduce below and which closely follows similar developments used before in the meson–meson interaction [7]. One defines the transition T-matrix as $T_{i,j}$ between the coupled channels which couple to certain quantum numbers. For instance, in the case of $\bar{K}N$ scattering studied in [6], the channels with zero charge are K^-p, $\bar{K}^0n$, $\pi^0\Sigma^0$, $\pi^+\Sigma^-$, $\pi^-\Sigma^+$, $\pi^0\Lambda$, $\eta\Lambda$, $\eta\Sigma^0$, $K^+\Xi^-$ and $K^0\Xi^0$. Unitarity in coupled channels is written as

$$\mathrm{Im}\, T_{i,j} = T_{i,\mathrm{l}}\rho_{\mathrm{l}}T^*_{\mathrm{l},j}, \tag{8}$$

where $\rho_i \equiv 2M_{\mathrm{l}}q_i/(8\pi W)$, with q_i the modulus of the c.m. three-momentum, and the subscripts i and j refer to the physical channels. This equation is most efficiently written in terms of the inverse amplitude as

$$\mathrm{Im}\; T^{-1}(W)_{ij} = -\rho(W)_i\delta_{ij}. \tag{9}$$

The unitarity relation in eq. (9) gives rise to a cut in the T-matrix of partial wave amplitudes, which is usually called the unitarity or right-hand cut. Hence one can write down a dispersion relation for $T^{-1}(W)$,

$$T^{-1}(W)_{ij} = -\delta_{ij}\left\{\widetilde{a}_i(s_0) + \frac{s-s_0}{\pi}\int_{s_i}^{\infty}\mathrm{d}s'\frac{\rho(s')_i}{(s'-s)(s'-s_0)}\right\} + \mathcal{T}^{-1}(W)_{ij}\ , \tag{10}$$

where s_i is the value of s at the threshold of channel i and $\mathcal{T}^{-1}(W)_{ij}$ indicates other contributions from local and pole terms, as well as crossed channel dynamics but *without* right-hand cut. These extra terms are taken directly from χPT after requiring the *matching* of the general result to the χPT expressions. Notice also that

$$g(s)_i = \widetilde{a}_i(s_0) + \frac{s - s_0}{\pi} \int_{s_i}^{\infty} \mathrm{d}s' \frac{\rho(s')_i}{(s' - s)(s' - s_0)} \tag{11}$$

is the familiar scalar loop integral.

One can further simplify the notation by employing a matrix formalism. Introducing the matrices $g(s) = \mathrm{diag}(g(s)_i)$, T and $\mathcal{T}$, the latter defined in terms of the matrix elements T_{ij} and $\mathcal{T}_{ij}$, the T-matrix can be written as

$$T(W) = [I - \mathcal{T}(W) \cdot g(s)]^{-1} \cdot \mathcal{T}(W) \tag{12}$$

which can be recast in a more familiar form as

$$T(W) = \mathcal{T}(W) + \mathcal{T}(W) g(s) T(W). \tag{13}$$

Now imagine that one is taking the lowest order chiral amplitude for the kernel $\mathcal{T}$ as done in [6]. Then the former equation is nothing but the Bethe–Salpeter equation with the kernel taken from the lowest-order Lagrangian and factorized on shell, the same approach followed in [5], where different arguments were used to justify the on-shell factorization of the kernel.

The on-shell factorization of the kernel, justified here with the N/D method, renders the set of coupled Bethe–Salpeter integral equations a simple set of algebraic equations.

4. Meson–baryon scattering

The low-energy $K^- N$ scattering and transition to coupled channels is one of the cases of successful application of chiral dynamics in the baryon sector. We rewrite eq. (7) in the more familiar form

$$T = V + V\, G\, T \tag{14}$$

with G the diagonal matrix given by the loop function of a meson and a baryon propagator.

The analytical expression for G_{l} can be obtained from [5] using a cut-off and from [6] using dimensional regularization. One has

$$G_{\mathrm{l}} = i \int \frac{\mathrm{d}^4 q}{(2\pi)^4} \frac{M_{\mathrm{l}}}{E_{\mathrm{l}}(\vec{q})} \frac{1}{\sqrt{s} - q^0 - E_{\mathrm{l}}(\vec{q}) + i\epsilon} \frac{1}{q^2 - m_{\mathrm{l}}^2 + i\epsilon} \tag{15}$$

in which M_{l} and m_{l} are the masses of the baryons and mesons respectively. In the dimensional regularization scheme this is given by

$$G_{\rm l} = i\,2M_{\rm l}\int \frac{{\rm d}^4q}{(2\pi)^4}\,\frac{1}{(P-q)^2-M_{\rm l}^2+i\epsilon}\,\frac{1}{q^2-m_{\rm l}^2+i\epsilon}$$
$$= \frac{2M_{\rm l}}{16\pi^2}\Bigg\{a_{\rm l}(\mu)+\ln\frac{M_{\rm l}^2}{\mu^2}+\frac{m_{\rm l}^2-M_{\rm l}^2+s}{2s}\ln\frac{m_{\rm l}^2}{M_{\rm l}^2}-2i\pi\frac{q_{\rm l}}{\sqrt{s}}$$
$$+\frac{q_{\rm l}}{\sqrt{s}}[\ln(s-(M_{\rm l}^2-m_{\rm l}^2)+2q_{\rm l}\sqrt{s})$$
$$+\ln(s+(M_{\rm l}^2-m_{\rm l}^2)+2q_{\rm l}\sqrt{s})$$
$$-\ln(s-(M_{\rm l}^2-m_{\rm l}^2)-2q_{\rm l}\sqrt{s})$$
$$-\ln(s+(M_{\rm l}^2-m_{\rm l}^2)-2q_{\rm l}\sqrt{s})]\Bigg\}, \tag{16}$$

where μ is the scale of dimensional regularization, $a_{\rm l}$ is the subtraction constant and $q_{\rm l}$ denotes the three-momentum of the meson or baryon in the centre-of-mass frame. We then look for poles of the transition matrix T in the complex $\sqrt{s}$ plane. The complex poles, $z_{\rm R}$, appear in unphysical Riemann sheets. We use the loop function of eq. (16) for energies below threshold and replace it above threshold with

$$G_{\rm l}^{\rm 2nd} = G_{\rm l} + 2i\,\frac{q_{\rm l}}{\sqrt{s}}\,\frac{M_{\rm l}}{4\pi}, \tag{17}$$

where the variables on the right-hand side of the above equation are evaluated in the first (physical) Riemann sheet. It is trivially verified that the same can be achieved by changing the sign of the complex-valued momentum $q_{\rm l}$ from positive to negative in the loop function $G_{\rm l}(z)$ of eq. (16) for the channels which are above threshold at an energy equal to ${\rm Re}(z)$. This we call the second Riemann sheet R_2.

5. Strangeness $S = -1$ sector

We take the K^-p state and all those that couple to it within the chiral scheme mentioned above. Hence we have a problem with ten coupled channels. The coupled sets of Bethe–Salpeter equations were solved in [5] using a cut-off momentum of 630 MeV in all channels. Changes in the cut-off can be accommodated in terms of changes in μ, the regularization scale in the dimensional regularization formula for $G_{\rm l}$, or in the subtraction constant $a_{\rm l}$. In order to obtain the same results as in [5] at low energies, we set μ equal to the cut-off momentum of 630 MeV (in all channels) and then find the values of the subtraction constants $a_{\rm l}$ such as to have $G_{\rm l}$ with the same value with the dimensional regularization formula and the cut-off formula at the $\bar{K}N$ threshold. For the purpose of this talk, let us recall that in [5] we obtain the $\Lambda(1405)$ resonance from the $\pi\Sigma$ spectrum and also evaluate the cross-sections for Kp to different channels, some of which are shown in figure 1.

6. Strangeness $S = 0$ sector

The strangeness $S = 0$ channel was also investigated using the Lippmann–Schwinger equation and coupled channels in [8]. The $N^*(1535)$ resonance was also generated

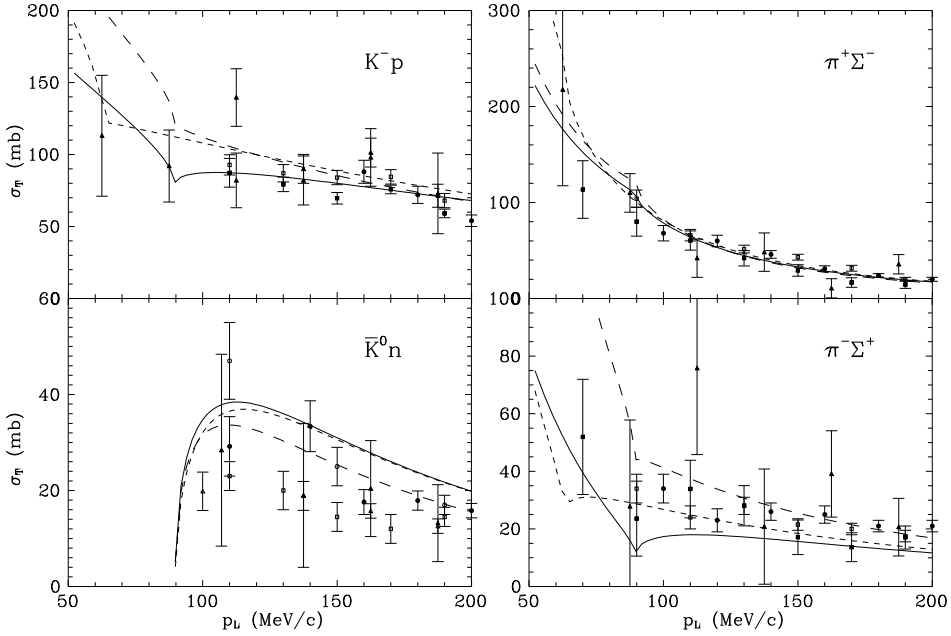

Figure 1. K^-p scattering cross-sections as functions of the K^- momentum in the lab frame: with the full basis of physical states (solid line), omitting the η channels (long-dashed line) and with the isospin-basis (short-dashed line). Taken from ref. [5].

dynamically within this approach. Subsequently work was done in this sector in [9] and [10] where the $N^*(1535)$ resonance was also generated. In [11], work along these lines was continued and improved by introducing the $\pi N \to \pi NN$ channels, which proved essential in reproducing the isospin 3/2 part of the πN amplitude, including the reproduction of the $\Delta(1620)$ resonance.

For total zero charge one has six channels in this case: π^-p, π^0n, ηn, $K^+\Sigma^-$, $K^0\Sigma^0$, and $K^0\Lambda$.

Details of the issues discussed in this paper can be seen in [12].

7. Poles of the T-matrix

The study of ref. [13] showed the presence of poles in eq. (12) around the $\Lambda(1405)$ and the $\Lambda(1670)$ for isospin $I = 0$ and around the $\Sigma(1620)$ in $I = 1$. The same approach in $S = -2$ leads to the resonance $\Xi(1620)$ [14] and in $S = 0$ to the $N^*(1535)$ [8,11]. One is thus tempted to consider the appearance of a singlet and an octet of meson–baryon resonances. Nevertheless, the situation is more complicated because indeed in the $SU(3)$ limit there are *two* octets and not just one, as we discuss below. The presence of these multiplets was already discussed in ref. [6] after obtaining a pole with $S = -1$ in the $I = 1$ channel, with mass around 1430 MeV, and two poles with $I = 0$, of masses around that of the $\Lambda(1405)$.

The appearance of a multiplet of dynamically generated mesons and baryons seems most natural once a state of the multiplet appears. Indeed, one must recall that the chiral Lagrangians are obtained from the combination of the octet of pseudoscalar mesons (the pions and partners) and the octet of stable baryons (the nucleons and partners). The $SU(3)$ decomposition of the combination of two octets tells us that

$$8 \otimes 8 = 1 \oplus 8_s \oplus 8_a \oplus 10 \oplus \overline{10} \oplus 27. \tag{18}$$

Thus, should we have a $SU(3)$ symmetric Lagrangian, one can expect e.g. one singlet and two octets of resonances, the symmetric and antisymmetric ones.

The lowest order of the meson–baryon chiral Lagrangian is exactly $SU(3)$ invariant if all the masses of the mesons, or equivalently the quark masses, are set equal. In ref. [13] the baryon masses take their physical values, although strictly speaking at the leading order in the chiral expansion they should be equal to M_0. For eq. (7) being $SU(3)$ symmetric, all the baryon masses M_i must be set equal as well. When all the meson and baryon masses are equal, and these common masses are employed in evaluating the $G_{\rm l}$ functions, together with equal subtraction constants $a_{\rm l}$, the T-matrix obtained from eq. (12) is also $SU(3)$ symmetric.

If we do such an $SU(3)$ symmetry approximation and look for poles of the scattering matrix, we find poles corresponding to the octets and singlet. The surprising result is that the two octet poles are degenerate as a consequence of the dynamics contained in the chiral Lagrangians. Indeed, if we evaluate the matrix elements of the transition potential V in a basis of $SU(3)$ states, we obtain something proportional to $V_{\alpha\beta} = \mathrm{diag}(6, 3, 3, 0, 0, -2)$ taking the following order for the irreducible representations: 1, 8_s, 8_a, 10, $\overline{10}$ and 27, with positive sign meaning attraction.

Hence we observe that the states belonging to different irreducible representations do not mix and the two octets appear degenerate. The coefficients in $V_{\alpha\beta}$ clearly illustrate why there are no bound states in the 10, $\overline{10}$ and 27 representations.

In practice, the same chiral Lagrangians allow for $SU(3)$ breaking. In the case of refs [5,13] the breaking appears because both in the V_{ij} transition potentials as in the $G_{\rm l}$ loop functions one uses the physical masses of the particles as well as different subtraction constants in $G_{\rm l}$, corresponding to the use of a unique cut-off in all the channels. In ref. [6] the physical masses are also used in the $G_{\rm l}$ functions, although these functions are evaluated with a unique subtraction constant as corresponds to the $SU(3)$ limit. In both approaches, physical masses are used to evaluate the $G_{\rm l}$ loop functions so that unitarity is fulfilled exactly and the physical thresholds for all channels are respected.

By following the approach of ref. [13] and using the physical masses of the baryons and the mesons, the position of the poles change and the two octets split apart in four branches, two for $I = 0$ and two for $I = 1$, as one can see in [15], which we reproduce in figure 2. In the figure we show the trajectories of the poles as a function of the parameter x that breaks the $SU(3)$ symmetry gradually up to the physical values. The dependence of masses and subtraction constants on the parameter x is given by

$$\begin{aligned} M_i(x) &= M_0 + x(M_i - M_0), \\ m_i^2(x) &= m_0^2 + x(m_i^2 - m_0^2), \\ a_i(x) &= a_0 + x(a_i - a_0), \end{aligned} \tag{19}$$

where $0 \leq x \leq 1$. In the calculation of figure 2, the values $M_0 = 1151$ MeV, $m_0 = 368$ MeV and $a_0 = -2.148$ are used.

The complex poles, $z_{\rm R}$, appear in unphysical sheets. In the present search we follow the strategy of changing the sign of the momentum $q_{\rm l}$ in the $G_{\rm l}(z)$ loop function for the channels which are open at an energy equal to ${\rm Re}(z)$.

The splitting of the two $I = 0$ octet states is very interesting. One moves to higher energies to merge with the $\Lambda(1670)$ resonance and the other one moves to lower energies to create a pole, quite well identified below the $\bar{K}N$ threshold, with a narrow width. On the other hand, the singlet also evolves to produce a pole at low energies with quite a large width.

We note that the singlet and the $I = 0$ octet states appear very close and what experiments actually see is a combination of the effect of these two resonances.

Similarly, as for the $I = 0$ octet states, we can see that one branch of the $I = 1$ states moves to higher energies while another moves to lower energies. The branch moving to higher energies finishes at what would correspond to the $\Sigma(1620)$ resonance when the physical masses are reached. The branch moving to lower energies fades away after a while when getting close to the $\bar{K}N$ threshold.

The model of ref. [6] reproduces qualitatively the same results, but the $I = 1$ pole also stays for $x = 1$. Nevertheless, in both approaches there is an $I = 1$ amplitude with an enhanced strength around the $\bar{K}N$ threshold. This amplitude has non-negligible consequences for reactions producing $\pi\Sigma$ pairs in that region. This has been illustrated, for instance, in ref. [16], where the photoproduction of the $\Lambda(1405)$ via the reaction $\gamma p \to K^+\Lambda(1405)$ was studied. It was shown that the different sign in the $I = 1$ component of the $|\pi^+\Sigma^-\rangle$, $|\pi^-\Sigma^+\rangle$ states leads, through interference between the $I = 1$ and the dominant $I = 0$ amplitudes, to different cross-sections

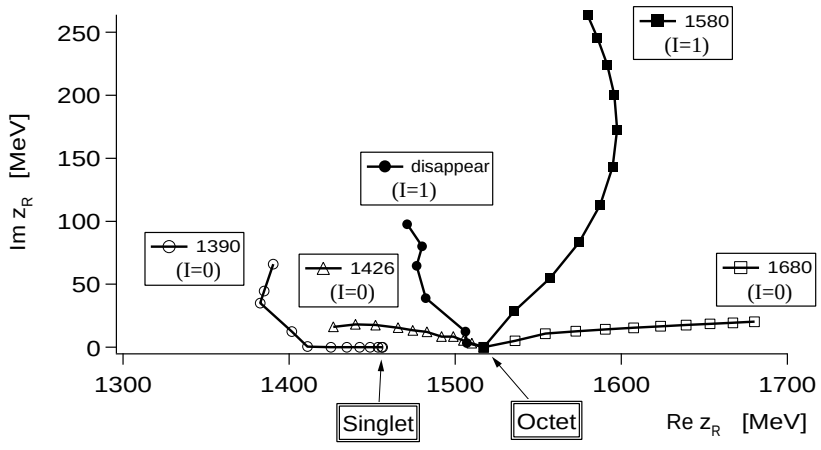

Figure 2. Trajectories of the poles in the scattering amplitudes obtained by changing the $SU(3)$ breaking parameter x gradually. At the $SU(3)$ symmetric limit ($x = 0$), only two poles appear, one is for the singlet and the other for the octet. The symbols correspond to the step size $\delta x = 0.1$. The results are from [15].

Table 1. Pole positions and couplings to $I = 0$ physical states from the model of ref. [13].

z_R	$1390 + 66i$		$1426 + 16i$		$1680 + 20i$	
$(I = 0)$	g_i	$\lvert g_i\rvert$	g_i	$\lvert g_i\rvert$	g_i	$\lvert g_i\rvert$
$\pi\Sigma$	$-2.5 - 1.5i$	2.9	$0.42 - 1.4i$	1.5	$-0.003 - 0.27i$	0.27
$\bar{K}N$	$1.2 + 1.7i$	2.1	$-2.5 + 0.94i$	2.7	$0.30 + 0.71i$	0.77
$\eta\Lambda$	$0.010 + 0.77i$	0.77	$-1.4 + 0.21i$	1.4	$-1.1 - 0.12i$	1.1
$K\Xi$	$-0.45 - 0.41i$	0.61	$0.11 - 0.33i$	0.35	$3.4 + 0.14i$	3.5

in the various charge channels, a fact that has been confirmed experimentally very recently [17].

Once the pole positions are found, one can also determine the couplings of these resonances to the physical states by studying the amplitudes close to the pole and identifying them with

$$T_{ij} = \frac{g_i g_j}{z - z_R}. \tag{20}$$

The couplings g_i are in general complex-valued numbers. In table 1, we summarize the pole positions and the complex couplings g_i obtained from the model of ref. [13] for isospin $I = 0$. The results with the model of [6] are qualitatively similar.

We observe that the second resonance with $I = 0$ couples strongly to the $\bar{K}N$ channel, while the first resonance couples more strongly to $\pi\Sigma$.

8. Influence of the poles on the physical observables

In a given reaction the $\Lambda(1405)$ resonance is always seen in $\pi\Sigma$ mass distribution. However, the $\Lambda(1405)$ can be produced through any of the channels in table 1. Hence, it is clear that, should there be a reaction which forces this initial channel to be $\bar{K}N$, then this would give more weight to the second resonance, R_2, and hence produce a distribution with a shape corresponding to an effective resonance narrower than the nominal one and at higher energy. Such a case indeed occurs in the reaction $K^-p \to \Lambda(1405)\gamma$ studied theoretically in ref. [18]. It was shown that since the K^-p system has a larger energy than the resonance, one has to lose energy emitting a photon prior to the creation of the resonance and this is effectively done by the Bremsstrahlung from the original K^- or the proton. Hence the resonance is initiated from the K^-p channel. This is also the case in the reaction $\gamma p \to K^*\Lambda(1405)$ which also has the $\Lambda(1405)$ initiated by $\bar{K}N$ through the vertex $\gamma \to K^*K$ [19]. In the next section, we report a recent experiment and its theoretical analysis that gives strong support to the idea of the two $\Lambda(1405)$ states.

9. Evidence for the two-pole structure of the Λ(1405) resonance

The recently measured reaction $K^- p \to \pi^0\pi^0\Sigma^0$ [20] allows us to test the two-pole nature of the Λ(1405). This process shows a strong similarity with the reaction $K^- p \to \gamma\Lambda(1405)$, where the photon is replaced by a π^0.

Our model for the reaction $K^- p \to \pi^0\pi^0\Sigma^0$ in the energy region of $p_{K^-} = 514$–750 MeV/c, as in the experiment [20], considers those mechanisms in which a π^0 loses the necessary energy to allow the remaining $\pi^0\Sigma^0$ pair to be on top of the Λ(1405) resonance. The first of such mechanisms is given in figure 3. In addition, analogy with the $\pi^- p \to K^0\pi\Sigma$ reaction, where $\pi\Sigma$ is also produced in the Λ(1405) region, demands that one also considers the mechanisms with a meson pole, involving the meson–meson amplitudes, as done in [21]. These mechanisms, together with the one in figure 3, are considered in the work of [22], which we summarize here, where the meson pole term was found to give a very small contribution.

Our calculations show that the process is largely dominated by the nucleon pole term shown in figure 3. As a consequence, the Λ(1405) thus obtained comes mainly from the $K^- p \to \pi^0\Sigma^0$ amplitude which, as mentioned above, gives the largest possible weight to the second (narrower) state.

In figure 4 our results for the invariant mass distribution for three different energies of the incoming K^- are compared to the experimental data. Symmetrization of the amplitudes produces a sizeable amount of background. At a kaon laboratory momentum of $p_K = 581$ MeV/c, this background distorts the Λ(1405) shape producing a cross-section in the lower part of M_I, while at $p_K = 714$ MeV/c, the strength of this background is shifted toward the higher M_I region. An ideal situation is found for momenta around 687 MeV/c, where the background sits below the Λ(1405) peak distorting its shape minimally. The peak of the resonance shows up at $M_I^2 = 2.02$ GeV^2 which corresponds to $M_I = 1420$ MeV, larger than the nominal Λ(1405), and in agreement with the predictions of ref. [15] for the location of the peak when the process is dominated by the $t_{\bar{K}N\to\pi\Sigma}$ amplitude. The apparent width from experiment is about 40–45 MeV, but a precise determination would be required to remove the background mostly coming from the 'wrong' $\pi^0\Sigma^0$ couples due to the indistinguishability of the two pions. A theoretical analysis permits extracting the pure resonant part by not symmetrizing the amplitude, and this is done in [22], where it is found that the width of the resonant part is $\Gamma = 38$ MeV, which is smaller than the nominal Λ(1405) width of 50 ± 2 MeV [23], obtained from the average of several experiments, and much narrower than the apparent width of about 60 MeV that one sees in the $\pi^- p \to K^0\pi\Sigma$ experiment [24], which also produces a distribution peaked at 1395 MeV. In order to illustrate the difference

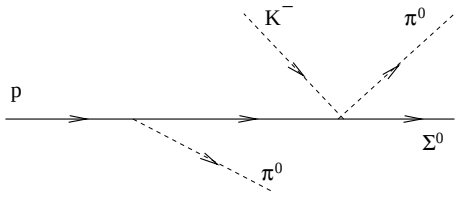

Figure 3. Nucleon pole term for the $K^- p \to \pi^0\pi^0\Sigma$ reaction.

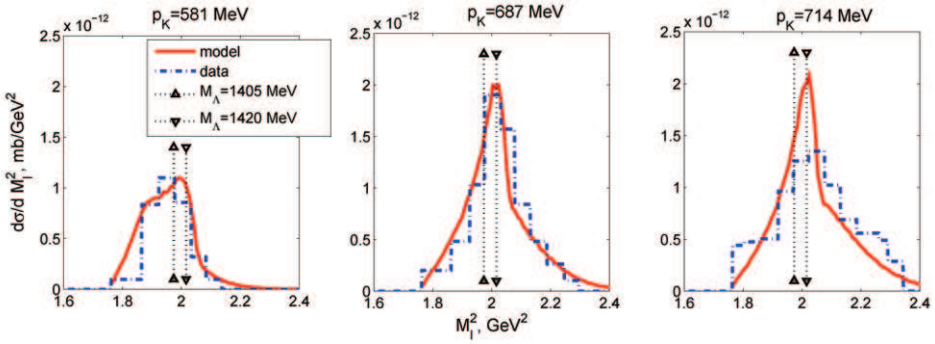

Figure 4. The $\pi^0\Sigma^0$ invariant mass distribution for three different initial kaon momenta.

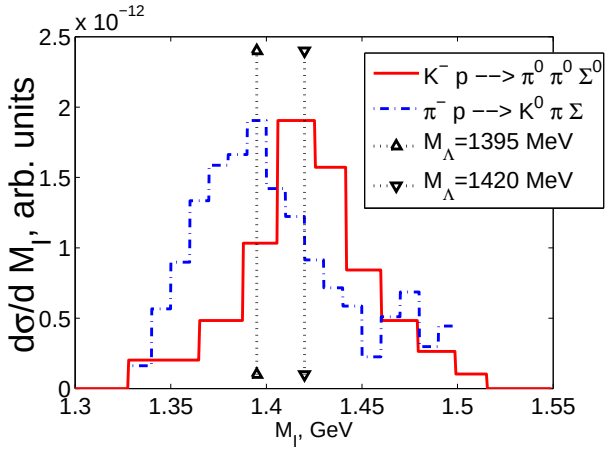

Figure 5. Two experimental shapes of $\Lambda(1405)$ resonance. See text for more details.

between the $\Lambda(1405)$ resonance seen in this latter reaction and in the present one, the two experimental distributions are compared in figure 5. We recall that the shape of the $\Lambda(1405)$ in the $\pi^- p \to K^0\pi\Sigma$ reaction was shown in ref. [21] to be largely built from the $\pi\Sigma \to \pi\Sigma$ amplitude, which is dominated by the wider, lower energy state.

The invariant mass distributions shown here are not normalized, as in experiment. But we can also compare our absolute values of the total cross-sections with those in ref. [20]. As shown in figure 6, our results are in excellent agreement with the data, in particular, for the three kaon momentum values whose corresponding invariant mass distributions have been displayed in figure 4.

In summary, we have shown, by means of a realistic model, that the $K^- p \to \pi^0\pi^0\Sigma^0$ reaction is particularly suited to study the features of the second pole of the $\Lambda(1405)$ resonance, since it is largely dominated by a mechanism in which a π^0 is emitted prior to the $K^- p \to \pi^0\Sigma^0$ amplitude, which is the one giving the largest

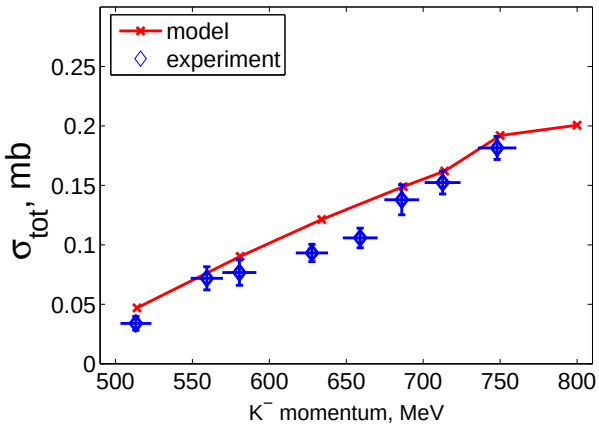

Figure 6. Total cross-section for the reaction $K^- p \to \pi^0\pi^0\Sigma^0$. Experimental data are taken from ref. [20].

weight to the second narrower state at higher energy. Our model has proved to be accurate in reproducing both the invariant mass distributions and integrated cross-sections seen in a recent experiment [20]. The study of the present reaction, complemental to the one in ref. [21] for the $\pi^- p \to K^0\pi\Sigma$ reaction, has shown that the different shapes of the $\Lambda(1405)$ resonance seen in these experiments can be interpreted in favour of the existence of two poles with the corresponding states having the characteristics predicted by the chiral theoretical calculations. Besides demonstrating once more the great predictive power of the chiral unitary theories, this combined study of the two reactions gives the first clear evidence of the two-pole nature of the $\Lambda(1405)$.

10. The interaction of the decuplet of baryons with the octet of mesons

Given the success of the chiral unitary approach in generating dynamically low-energy resonances from the interaction of the octets of stable baryons and the pseudoscalar meson, in [25], the interaction of the decuplet of $3/2^+$ with the octet of pseudoscalar mesons was studied and shown to lead to many states which were associated to experimentally well-established $3/2^-$ resonances.

The lowest-order chiral Lagrangian for the interaction of the baryon decuplet with the octet of pseudoscalar mesons is given by [26]

$$L = -(i\bar{T}^\mu D_\nu \gamma^\nu T_\mu - m_T \bar{T}^\mu T_\mu), \tag{21}$$

where T^μ_{abc} is the spin decuplet field and D^ν the covariant derivative given in [26]. The identification of the physical decuplet states with T^μ_{abc} can be seen in [27], where a detailed study of this interaction and the resonances generated can be seen. The study is done along the lines of the former sections, looking for poles in the second Riemann sheet of the complex plane, the coupling of the resonances to

the different channels and the stability of the results with respect to variations of the input parameter, which in our case is just the subtraction constant, a. This allows the association of the resonances found to existing states of the particle data book, and the prediction of new ones. Details of the results obtained can be seen in figure 7.

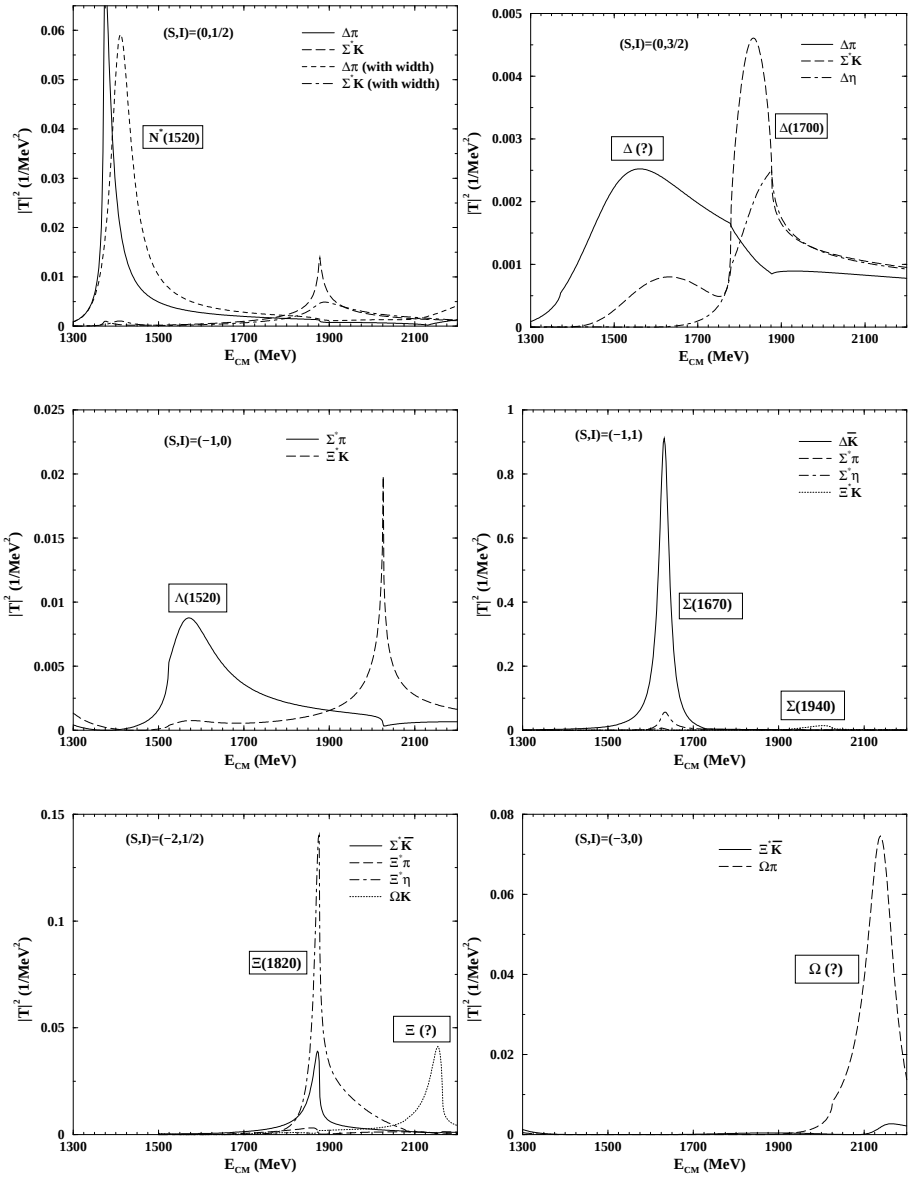

Figure 7. Resonances obtained from the interaction of the octet of mesons with the decuplet of baryons.

Another interesting result is the generation of an exotic state of $S = 1$ and $I = 1$ which is generated by the interaction of the ΔK channels and stands as a ΔK resonance. The pole appears in a Riemann sheet below threshold when the sign of the momentum is also changed, but it leads to a ΔK amplitude which accumulates strength close to threshold and produces a broad peak in the cross-section in contrast to the $I = 2$ cross-section which is much smaller and very smooth. However, the situation is not completely clear since as shown in [28], the results are very sensitive to changes in the input and the mere change of f to f_K makes the pole disappear. It is not clear what would happen if higher-order terms of the interaction were taken into account, and for the moment it remains as an interesting observation.

11. Chiral coupled channel dynamics of the $\Lambda(1520)$ and the $K^- p \to \pi^0\pi^0\Lambda$ reaction

In [29], a refinement of the approach discussed above has been done including the $\bar{K}N$ and $\pi\Sigma$ decay channels of the $\Lambda(1520)$ and fine-tuning the subtraction constant in the g function, such that a good agreement with the position and width of the $\Lambda(1520)$ is attained. With this new information one can study the reaction $K^- p \to \pi^0\pi^0\Lambda$ by using the mechanisms of figure 8 which provides the dominant contribution to the reaction at energies close to the $\Lambda(1520)$. At higher energies of the experiment of [30] one finds that the mechanisms depicted in figure 9 provide a contribution that helps bring the theory and experiment in good agreement as can be seen in figure 10. One can see in the figure that up to 575 MeV/c of momentum of the K^-, the mechanism based on the strong coupling of the $\Lambda(1520)$ to the $\pi\Sigma(1385)$ channel is largely dominant and provides the right strength of the cross-section. Obviously, it would be most interesting to investigate the region of lower energies of the K^- in order to see if the predictions done by the theory are accurate.

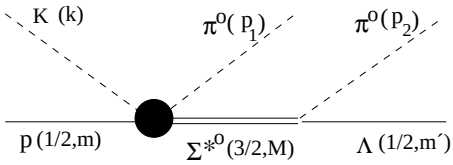

Figure 8. Scheme for $K^- p \to \pi^0\Sigma^{*0}(1385) \to \pi^0\pi^0\Lambda(1116)$. The blob indicates the unitarized vertex.

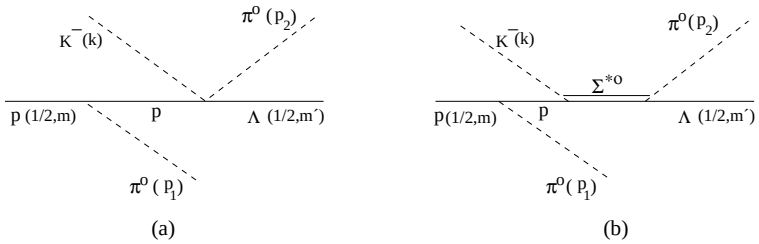

Figure 9. A conventional scheme for $K^- p \to \pi^0\pi^0\Lambda$.

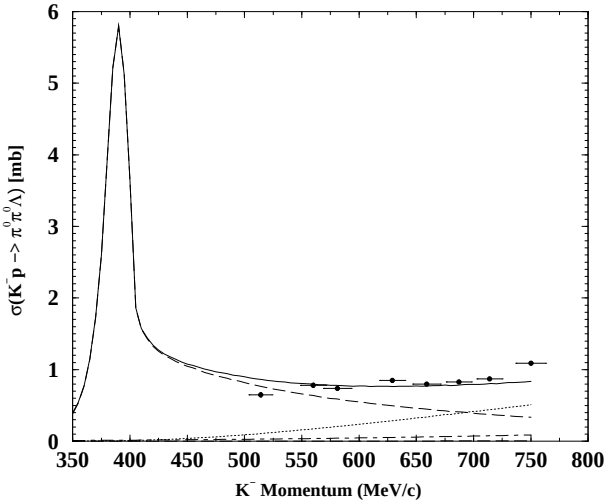

Figure 10. Cross-section as a function of the K^- momentum. The dot–dashed and dotted lines are the contributions of the diagrams of figures 9a and 9b respectively. The dashed line shows the cross-section with figure 8 only and the solid line for a coherent sum of all these diagrams.

In figure 11, we compare the predictions for the invariant mass distribution of $\pi^0\Lambda$ with experiment. The shape of the $\Sigma(1385)$ is clearly visible, although, as in §9, the symmetry of the pions induces a background from the 'wrong' $\pi^0\Lambda$ couples. The agreement of the theory and experiment gives a strong support to the idea of the $\Lambda(1520)$ being a quasi-bound state of $\pi\Sigma(1385)$, but a stronger support would be provided by the measurements at lower energy showing the predicted excitation of the $\Lambda(1520)$ resonance.

12. $\bar{K}$ in nuclei

Next we address the properties of the $\bar{K}$ in the nuclear medium which have been studied in [31]. The work is based on the elementary $\bar{K}N$ interaction which has been discussed above, using a coupled channel unitary approach with chiral Lagrangians.

The coupled channel formalism requires to evaluate the transition amplitudes between the different channels that can be built from the meson and baryon octets. For K^-p scattering there are 10 such channels, namely K^-p, $\bar{K}^0n$, $\pi^0\Lambda$, $\pi^0\Sigma^0$, $\pi^+\Sigma^-$, $\pi^-\Sigma^+$, $\eta\Lambda$, $\eta\Sigma^0$, $K^+\Xi^-$ and $K^0\Xi^0$. In the case of K^-n scattering the coupled channels are: K^-n, $\pi^0\Sigma^-$, $\pi^-\Sigma^0$, $\pi^-\Lambda$, $\eta\Sigma^-$ and $K^0\Xi^-$.

In order to evaluate the $\bar{K}$ self-energy in the medium, one needs to first include the medium modifications in the $\bar{K}N$ amplitude, $T^{\alpha}_{\rm eff}$ ($\alpha = \bar{K}p, \bar{K}n$), and then perform the integral over the nucleons in the Fermi sea:

$$\Pi^s_{\bar{K}}(q^0,\vec{q},\rho) = 2\int \frac{\mathrm{d}^3p}{(2\pi)^3} n(\vec{p}) \left[T^{\bar{K}p}_{\rm eff}(P^0,\vec{P},\rho) + T^{\bar{K}n}_{\rm eff}(P^0,\vec{P},\rho)\right]. \quad (22)$$

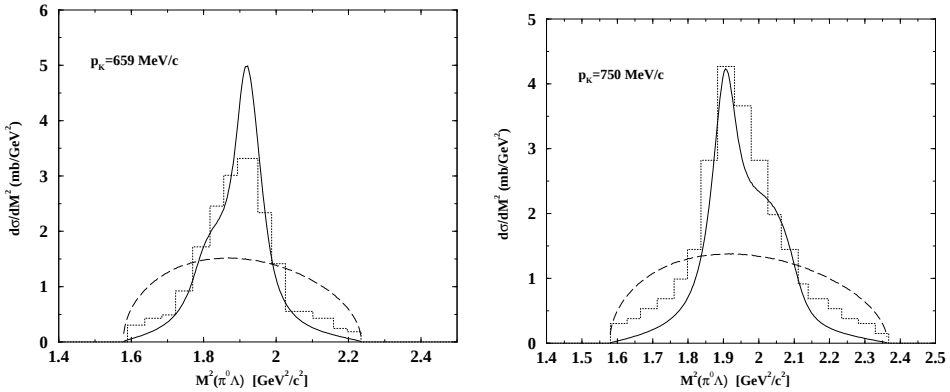

Figure 11. $\mathrm{d}\sigma/\mathrm{d}M^2$ as a function of the invariant mass of $\pi^0\Lambda$ for two values of the K^- momentum in CM; left: 659 MeV and right: 750 MeV. Solid lines represent our results. The dotted histograms are the experimental results from [30] normalized to the total experimental cross-section. The dashed lines indicate the phase space normalized to the theoretical cross-section.

The values $(q^0, \vec{q})$ stand now for the energy and momentum of the $\bar{K}$ in the lab frame, $P^0 = q^0 + \varepsilon_N(\vec{p})$, $\vec{P} = \vec{q} + \vec{p}$ and ρ is the nuclear matter density.

We also include a p-wave contribution to the $\bar{K}$ self-energy coming from the coupling of the $\bar{K}$ meson to hyperon–nucleon hole (YN^{-1}) excitations, with $Y = \Lambda, \Sigma, \Sigma^*(1385)$. The vertices MBB' are easily derived from the D and F terms of eq. (1). The explicit expressions can be seen in [31].

At this point it is interesting to recall three different approaches to the question of the $\bar{K}$ self-energy in the nuclear medium. The first interesting realization was the one in [32–34], where the Pauli blocking in the intermediate nucleon states induced a shift of the $\Lambda(1405)$ resonance to higher energies and a subsequent attractive $\bar{K}$ self-energy. The work of [35] introduced a novel and interesting aspect, the self-consistency. Consideration of Pauli blocking required a higher energy to produce the resonance, but having a smaller kaon mass led to an opposite effect, and as a consequence the position of the resonance was brought back to the free position. Yet, a moderate attraction on the kaons still resulted, but weaker than anticipated from the former work. The work of [31] introduces some novelties. It incorporates the self-consistent treatment of the kaons done in [35] and in addition it also includes the self-energy of the pions, which are let to excite ph and Δh components. It also includes the mean-field potentials of the baryons. The obvious consequence of the work of [31] is that the spectral function of the kaons gets much wider than in the two former approaches because one includes new decay channels for the $\bar{K}$ in nuclei.

In the work of [36], the kaon self-energy discussed above has been used for the case of kaonic atoms, where there are abundant data to test the theoretical predictions. One uses the Klein–Gordon equation and obtains two families of states. One family corresponds to the atomic states, some of which are those already measured, and which have energies around or below 1 MeV and widths of about a few hundred KeV or smaller. The other family corresponds to states which are

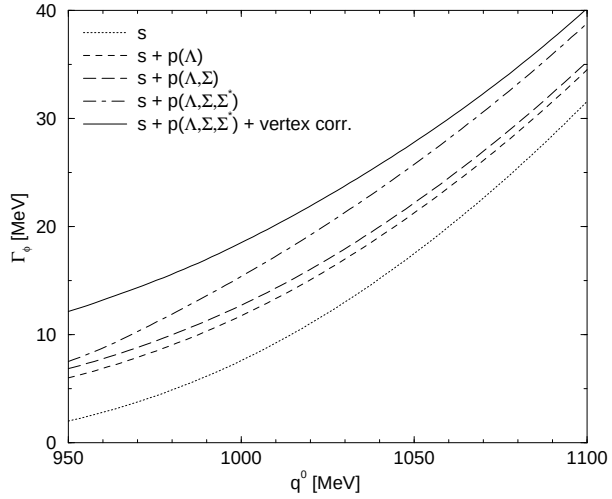

Figure 12. ϕ width at $\rho = \rho_0$.

nuclear deeply bound states, with energies of 10 MeV or more and widths around 100 MeV.

With the K^- many-body decay channels included in our approach, the resulting widths of the deeply bound K^- states (never bound by more than 50 MeV) are very large (of the order of 100 MeV) and, hence, there is no room for narrow deeply bound K^- states which appear in some oversimplified theoretical approaches. A recent phenomenological work [37] considering the $K^-NN \to \Lambda N\Sigma N$ nuclear kaon absorption channels, which are also incorporated in [31], reaches the conclusion that in the unlikely case, there would be deeply bound kaonic atoms and they should have necessarily a large width.

13. ϕ Decay in nuclei

Let us say a few words about the ϕ decay in nuclei. The work reported in [38] follows closely the lines of [39,40], however, it uses the updated $\bar{K}$ self-energies of [31]. In the present case the ϕ decays primarily in $K\bar{K}$, but these kaons can now interact with the medium as discussed previously. For the K self-energy, since the KN interaction is not too strong and there are no resonances, the $t\rho$ approximation is sufficient. In figure 12, we show the results for the ϕ width at $\rho = \rho_0$ as a function of the mass of ϕ, separating the contribution from the different channels. What we observe is that the consideration of the s-wave $\bar{K}$-self-energy is responsible for a sizeable increase of the width in the medium, but the p-wave is also relevant, particularly the Λh excitation and the $\Sigma^* h$ excitation. It is also interesting to note that the vertex corrections [41] (Yh loops attached to the ϕ decay vertex) are now present and do not cancel off-shell contributions like in the case of the scalar mesons. Their contribution is also shown in the figure and has about the same strength as the other p-wave contributions. The total width of ϕ that we obtain is about 22 MeV at $\rho = \rho_0$, about a factor two smaller than the one obtained in [39,40]. A

Table 2. $(B,-\Gamma/2)$ for η-nucleus bound states calculated with the energy-dependent potential. Units in MeV

	^{12}C	^{24}Mg	^{27}Al	^{28}Si	^{40}Ca	^{208}Pb
$1s$	(−9.71, −17.5)	(−12.57, −16.7)	(−16.65, −17.98)	(−16.78, −17.93)	(−17.88, −17.19)	(−21.25,−15.88)
$1p$			(−2.90, −20.47)	(−3.32, −20.35)	(−7.04, −19.30)	(−17.19,−16.58)
$1d$						(−12.29,−17.74)
$2s$						(−10.43,−17.99)
$1f$						(−6.64,−19.59)
$2p$						(−3.79,−19.99)
$1g$						(−0.33,−22.45)

recent evaluation of the ϕ self-energy in the medium [42] similar to that of [38], in which the real part is also evaluated, leads to a width which is about 20% larger than that of [38]. An important finding from all these works is, however, the nearly one order of magnitude increase of the width with respect to the free one.

14. η Self-energy and η bound in nuclei

The method of Ramos and Oset [31] has also been used recently to determine the η self-energy in the nuclear medium [43]. One obtains a potential at threshold of the order of $(-54\ -i29)$ MeV at normal nuclear matter, but it also has a strong energy dependence due to the proximity of the $N^*(1535)$ resonance and its appreciable modification in the nuclear medium.

To compute the η-nucleus bound states, we solve the Klein–Gordon equation (KGE) with the η self-energy, $\Pi_\eta(k^0,r) \equiv \Pi_\eta(k^0,\vec{0},\rho(r))$, obtained using the local density approximation. We then have

$$[-\vec{\nabla}^2 + \mu^2 + \Pi_\eta(\mathrm{Re}[E],r)]\Psi = E^2\Psi, \tag{23}$$

where μ is the η-nucleus reduced mass, the real part of E is the total meson energy, including its mass, and the imaginary part of E, with opposite sign, is the half-width $\Gamma/2$ of the state. The binding energy $B<0$ is defined as $B = \mathrm{Re}[E] - m_\eta$.

The results from [44] are shown in table 2 for the energy-dependent potential. On the other hand, we see that the half-widths of the states are large, in fact larger than the binding energies or the separation energies between neighbouring states.

With the results obtained here it looks like the chances to see distinct peaks corresponding to η bound states are not too big.

On the other hand, one can look at the results with a more optimistic view if one simply takes into account that experiments searching for these states might not see them as peaks, but they should see some clear strength below threshold in the η production experiments. The range by which this strength would go into the bound region would measure the combination of half-width and binding energy. Even if this is less information than the values of the energy and width of the states, it

is by all means a relevant information to gain some knowledge on the η nucleus optical potential.

15. Experiments to determine the ϕ width in the medium

Recently there has been an experiment [45] to determine the width of ϕ in nuclei. Unlike other experiments proposed which aim at determining the width from the K^+K^- invariant mass distribution and which look extremely difficult [47,48], the experiment done in Spring8/Osaka uses a different philosophy, since it looks at the A dependence of the ϕ photoproduction cross-section. The idea is that ϕ gets absorbed in the medium with a probability per unit length equal to $-\mathrm{Im}\,\Pi/q$, where Π is the ϕ self-energy in the medium ($\Gamma = -\mathrm{Im}\,\Pi/\omega_\phi$). The bigger the nucleus the more ϕ gets absorbed and there is a net diversion from the A proportionality expected from a photonuclear reaction. The method works and one obtains a ϕ width in the medium which is given in [45] in terms of a modified ϕN cross-section in the nucleus sizeably larger than the free one. Prior to these experimental results there is a theoretical calculation in [46] adapted to the set up of the experiment of [45], based on the results for the ϕ self-energy reported above. The results agree only qualitatively with the experimental ones, the latter ones indicating that the ϕ self-energy in the medium could be even larger than the calculated one. However, although it has been fairly taken into account in the experimental analysis, there is a problem in the reaction of [45], since there is a certain contamination of coherent ϕ production which blurs the interpretation of the data.

This can be seen in figure 13 taken from [45]. In figure 13b, the cross-sections are normalized to the cross-section of ^{7}Li.

There is an apparent discrepancy of the experimental results with the theory. Yet, one could assume that there is much contamination of coherent ϕ production in ^{7}Li, which certainly contains the largest amount since coherent production is thwarted by the nuclear form factors, much smaller in heavy nuclei for the momentum transfers involved in the reaction. If one removes the ^{7}Li datum and normalizes all the cross-sections to ^{12}C, then the agreement between theory and experiment is much better.

In order to use the same idea of the A dependence and get rid of the coherent ϕ production, a new reaction has been suggested in [49] which could be implemented in a facility like COSY. The idea is to measure the ϕ production cross-section in different nuclei through the reaction

$$pA \to \phi X. \tag{24}$$

The calculation is done assuming one-step production, and two-step production with a nucleon or Δ in the intermediate states, allowing for the loss of ϕ flux as ϕ is absorbed in its way out of the nucleus. Predictions for the cross-sections normalized to the one of ^{12}C are shown in figure 14 where it is shown that with a precision of 10% in the experimental ratios one could disentangle between the different curves in the figure and could easily determine if the width is one time, two times etc., the width determined in refs [38,42] which is about 27 MeV for normal nuclear matter density. An experiment of this type can be easily performed in the COSY facility, where hopefully it will be done in the near future.

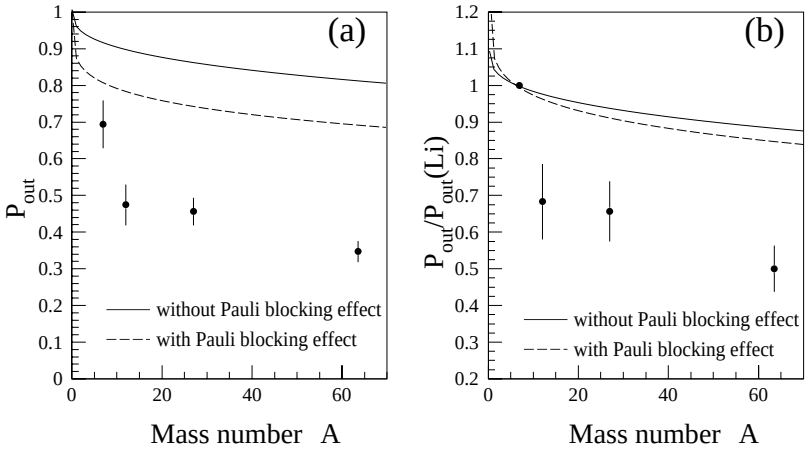

Figure 13. (**a**) The probability $P_{\rm out}=\sigma_A/(A\sigma_N)$. The overall normalization error (18%) is not included. The solid and dashed curves show the theoretical calculations given by Cabrera *et al* [46] without and with Pauli blocking correction for the ϕ meson scattering angle in the laboratory frame of 0°, respectively. (**b**) The ratio $P_{\rm out}/P_{\rm out}({\rm Li})$. The solid and dashed curves show the theoretical calculations as in (a). The data (filled circles) are from ref. [45].

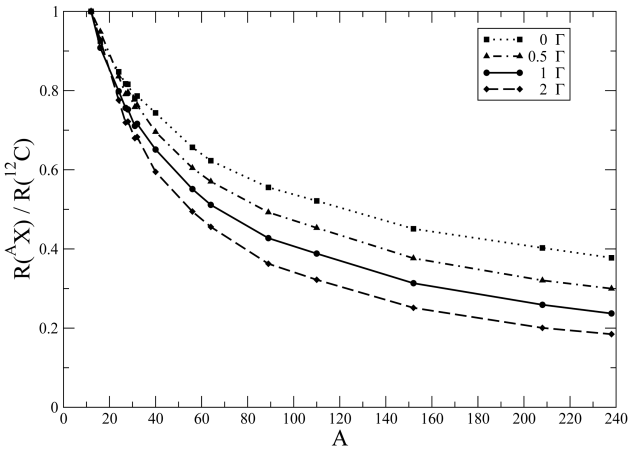

Figure 14. Ratio of the nuclear cross-section normalized to ^{12}C for $T_p = 2.83$ GeV multiplying the ϕ width in the medium, Γ around 27 MeV, by different factors.

16. Conclusions

The use of chiral Lagrangians for the meson–baryon interaction and the unitary extensions of chiral perturbation theory have given us an opportunity to face a large number of problems which were restricted to the standard perturbation techniques. It has opened the door to the study of many baryonic resonances which qualify

well as dynamically generated resonances, or quasi-bound states of meson–baryon. Thanks to this, a quantitative description of the meson–baryon interaction at intermediate energies is now possible and with this, an important systematics has been introduced in the many-body problem to face issues on the renormalization of hadron properties in the nuclear medium. The constructed scheme is rather powerful and allows to make predictions which consecutive experiments are proving right. Two of these predictions, the two states for the $\Lambda(1405)$, and the nature of the $\Lambda(1520)$ as a quasi-bound state of $\pi\Sigma(1385)$, have found strong support from two very recent experiments. Ongoing experiments on the ϕ width in the nuclear medium should soon provide reliable information on this so long sought important magnitude. The final conclusion is that chiral dynamics is a key ingredient that allows a unified description of much of the hadronic world at low and intermediate energies.

Acknowledgments

DC and LR acknowledge support from the Ministerio de Educación y Ciencia. This work is partly supported by the Spanish CSIC and JSPS Collaboration, the DGICYT contract number BFM2003-00856, and the E.U. EURIDICE network contract no. HPRN-CT-2002-00311. This research is part of the EU Integrated Infrastructure Initiative Hadron Physics Project under contract number RII3-CT-2004-506078.

References

[1] J Gasser and H Leutwyler, *Nucl. Phys.* **B250**, 465, 517, 539 (1985)
[2] U G Meissner, *Rep. Prog. Phys.* **56**, 903 (1993)
V Bernard, N Kaiser and U G Meissner, *Int. J. Mod. Phys.* **E4**, 193 (1995)
[3] G Ecker, *Prog. Part. Nucl. Phys.* **35**, 1 (1995)
[4] N Kaiser, P B Siegel and W Weise, *Nucl. Phys.* **A594**, 325 (1995), arXiv:nucl-th/9505043
[5] E Oset and A Ramos, *Nucl. Phys.* **A635**, 99 (1998)
[6] J A Oller and U G Meissner, *Phys. Lett.* **B500**, 263 (2001)
[7] J A Oller and E Oset, *Phys. Rev.* **D60**, 074023 (1999)
[8] N Kaiser, P B Siegel and W Weise, *Phys. Lett.* **B362**, 23 (1995)
[9] J C Nacher, A Parreno, E Oset, A Ramos, A Hosaka and M Oka, *Nucl. Phys.* **A678**, 187 (2000), arXiv:nucl-th/9906018
[10] J Nieves and E Ruiz Arriola, *Phys. Rev.* **D64**, 116008 (2001)
[11] T Inoue, E Oset and M J Vicente Vacas, *Phys. Rev.* **C65**, 035204 (2002), arXiv:hep-ph/0110333
[12] J A Oller, E Oset and A Ramos, *Prog. Part. Nucl. Phys.* **45**, 157 (2000)
[13] E Oset, A Ramos and C Bennhold, *Phys. Lett.* **B527**, 99 (2002), Erratum, *Phys. Lett.* **B530**, 260 (2002)
[14] A Ramos, E Oset and C Bennhold, *Phys. Rev. Lett.* **89**, 252001 (2002)
[15] D Jido, J A Oller, E Oset, A Ramos and U G Meissner, *Nucl. Phys.* **A725**, 181 (2003)
[16] J C Nacher, E Oset, H Toki and A Ramos, *Phys. Lett.* **B455**, 55 (1999)

[17] J K Ahn *et al*, *Proceedings of the XVI Particles and Nuclei International Conference* (PANIC02), edited by K Imai, T Kishimodo and H Toki, *Nucl. Phys.* **A721**, 715 (2003)
[18] J C Nacher, E Oset, H Toki and A Ramos, *Phys. Lett.* **B461**, 299 (1999)
[19] T Hyodo, A Hosaka, M J Vicente Vacas and E Oset, *Phys. Lett.* **B593**, 75 (2004)
[20] Crystall Ball Collaboration: S Prakhov *et al*, *Phys. Rev.* **C70**, 034605 (2004)
[21] T Hyodo, A Hosaka, E Oset, A Ramos and M J Vicente Vacas, *Phys. Rev.* **C68**, 065203 (2003), arXiv:nucl-th/0307005
[22] V K Magas, E Oset and A Ramos, *Phys. Rev. Lett.* **95**, 052301 (2005), arXiv:hep-ph/0503043
[23] Particle Data Group: K Hagiwara *et al*, *Phys. Rev.* **D66**, 010001 (2002)
[24] D W Thomas, A Engler, H E Fisk and R W Kraemer, *Nucl. Phys.* **B56**, 15 (1973)
[25] E E Kolomeitsev and M F M Lutz, *Phys. Lett.* **B585**, 243 (2004)
[26] E Jenkins and A V Manohar, *Phys. Lett.* **B259**, 353 (1991)
[27] S Sarkar, E Oset and M J Vicente Vacas, *Nucl. Phys.* **A750**, 294 (2005), arXiv:nucl-th/0407025
[28] S Sarkar, E Oset and M J Vicente Vacas, *Eur. Phys. J.* **A24**, 287 (2005), arXiv:nucl-th/0404023
[29] S Sarkar, E Oset and M J Vicente Vacas, *Phys. Rev.* **C72**, 015206 (2005), arXiv:hep-ph/0503066
[30] S Prakhov *et al*, *Phys. Rev.* **C69**, 042202 (2004)
[31] A Ramos and E Oset, *Nucl. Phys.* **A671**, 481 (2000)
[32] V Koch, *Phys. Lett.* **B337**, 7 (1994)
[33] T Waas, N Kaiser and W Weise, *Phys. Lett.* **B365**, 12 (1996); **B379**, 34 (1996)
[34] T Waas and W Weise, *Nucl. Phys.* **A625**, 287 (1997)
[35] M Lutz, *Phys. Lett.* **B426**, 12 (1998)
[36] S Hirenzaki, Y Okumura, H Toki, E Oset and A Ramos, *Phys. Rev.* **C61**, 055205 (2000)
[37] J Mares, E Friedman and A Gal, *Phys. Lett.* **B606**, 295 (2005), arXiv:nucl-th/0407063
[38] E Oset and A Ramos, *Nucl. Phys.* **A679**, 616 (2001)
[39] F Klingl, T Waas and W Weise, *Phys. Lett.* **B431**, 254 (1998)
[40] F Klingl, N Kaiser and W Weise, *Nucl. Phys.* **A624**, 527 (1997)
[41] M Herrmann, B L Friman and W Noeremberg, *Nucl. Phys.* **A560**, 411 (1993)
[42] D Cabrera and M J Vicente Vacas, *Phys. Rev.* **C67**, 045203 (2003), arXiv:nucl-th/0205075
[43] T Inoue and E Oset, *Nucl. Phys.* **A710**, 354 (2002)
[44] C Garcia-Recio, J Nieves, T Inoue and E Oset, *Phys. Lett.* **B550**, 47 (2002), arXiv:nucl-th/0206024
[45] J K Ahn *et al*, *Phys. Lett.* **B608**, 215 (2005), arXiv:nucl-ex/0411016
[46] D Cabrera, L Roca, E Oset, H Toki and M J V Vacas, *Nucl. Phys.* **A733**, 130 (2004), arXiv:nucl-th/0310054
[47] E Oset, M J Vicente Vacas, H Toki and A Ramos, *Phys. Lett.* **B508**, 237 (2001), arXiv:nucl-th/0011019
[48] P Muhlich, L Alvarez-Ruso, O Buss and U Mosel, *Phys. Lett.* **B595**, 216 (2004), arXiv:nucl-th/0401042
[49] V K Magas, L Roca and E Oset, *Phys. Rev.* **C71**, 065202 (2005), arXiv:nucl-th/0403067